Contributions to Geophysics and Geodesy Vol. 53/3, 2023 (225–240)

Fingerprinting the North-Atlantic and Arctic oscillation signals in rainfall and new snowpack in the western Carpathian Mountains

Milan ONDERKA[1,2,*], Jozef PECHO[2,3]

[1] Earth Science Institute of the Slovak Academy of Sciences, Dept. of Atmospheric Physics, Dúbravská cesta 9, Bratislava, SK-814 38, Slovak Republic

[2] Slovak Hydrometeorological Institute, Jeséniova 17, Bratislava, SK-833 15, Slovak Republic

[3] Faculty of Mathematics, Physics and Informatics, Comenius University, Bratislava, SK-842 48, Slovak Republic

Abstract: Time-varying relationships between two atmospheric oscillation modes and precipitation (rainfall and snow) in the western portion of the Carpathian Mountains and the northern part of the Pannonian Plain are investigated in this paper. The Arctic Oscillation (AO) and the North Atlantic Oscillation (NAO) modes were used to explain the intra-annual variability of monthly rainfall totals and new snow over a 36-year period (1981–2017) observed at a dense network of 177 rain gauges and 33 snow rods located throughout the investigated area, respectively. The Continuous Wavelet Transform (CWT) was deployed as a band-pass filter to quantify the spectral coherence and attribution (based on signal-to-noise ratio) of the NAO and AO modes to the precipitation variability. The temporal and spatial patterns of NAO and AO-related signal variance in monthly rainfall totals and fresh snowpack were evaluated on seasonal and monthly bases. The NAO mode explained the major historically observed snow calamities, such as the snowy cold spell of January 1985 that hit central and southern Europe, bringing heavy snowfall to the investigated region and many other parts of Europe. This event was the beginning of a prolonged cold wave in Europe, with extremely low air temperatures across the continent. Our analyses showed that the AO mode appears to have only a limited effect on the overall variability of new snowpack in late winter. The attribution of NAO and AO modes to the variability of monthly rainfall totals is less pronounced compared to new snowpack.

Key words: signal-to-noise ratio, NAO, AO, Carpathians, precipitation, rainfall, snowpack

1. Introduction

Rainfall and its temporal variability are important factors in the development of droughts and floods. Long-distance relationships between two or

*corresponding author, e-mail: milan.onderka@savba.sk

doi: 10.31577/congeo.2023.53.3.4

more climate phenomena (known as teleconnections) have been the subject of extensive research over the past decades (*Rust et al., 2021; Tabari and Willems, 2018; Peings et al., 2017; Casanueva et al., 2014; Fye et al., 2006; Feldstein, 2000*). Teleconnections have been related to air temperature, precipitation, snow cover, and runoff (*Wang et al., 2017; Casanueva et al., 2014; Brands et al., 2014*).

Several teleconnection patterns in the Northern Hemisphere have been proposed to facilitate our understanding of pressure anomalies over the Northern Atlantic and the Arctic Ocean and their impact on precipitation extremes in the Northern Hemisphere. Perhaps the most frequently examined relationship between precipitation and climate system anomalies is the North-Atlantic Oscillation (NAO). NAO is often used as an indicator of hydrometeorological conditions due to its leading control over wintertime precipitation (*Rust et al., 2021*). *Bednorz and Wibig (2008)* investigated the influence of NAO on snowpack depth. *Tabari and Willems (2018)* found that in Europe, the correlation between the anomalies of extreme precipitation and NAO ranges from 2% to 21%. The area over which the correlation between the anomalies of extreme precipitation and NAO is significant ranges from 2% in spring to 21% in winter. Although the NAO is dynamically active mostly during the winter season, summer NAO is a weaker counterpart with an inverse effect on precipitation across Europe (*Tabari and Willems, 2018*).

Similarly to the NAO, the Arctic Oscillation (AO) has been previously shown to have a similar yet weaker effect on winter precipitation in Europe (*Tabari and Willems, 2018*). Positive phases of AO are associated with extreme manifestations of rainfall, especially in the northern parts of Europe, whereas the negative phase is associated with extreme precipitation in the Mediterranean area (*Tabari and Willems, 2018*). Yet, there are also other studies that support the potential impacts of AO and NAO on European precipitation patterns and extreme precipitation events. For example, *Seager et al. (2020)* described the mechanisms of winter precipitation variability in the European-Mediterranean region and associated them with the North Atlantic oscillation. A recent study by *Tabari and Willems (2018)* showed that concurrent and seasonally delayed impacts of the NAO and AO on extreme precipitation in Europe. They found that summer extremes in precipitation are affected by the preceding winter NAO anomalies. This has

direct implications for water resources forecasting, understanding hydrological variability over seasonal and annual time-scales (*Rust et al., 2021*), and adaptation planning and preparedness for natural disasters arising from extreme precipitation (*Tabari and Willems, 2018*).

Every effort to identify a desired signal in a noisy background requires the application of signal processing techniques. Most attempts to identify "fingerprints" of NAO and AO in observed time series rely on the use of Spearman and Pearson correlation techniques (*Ríos-Cornejo et al., 2015; Tabari and Willems, 2018*). Unfortunately, Pearson correlation makes it impossible to identify the exact timing when NAO or AO signals correlate with the hydrometeorological observations. Rather than focusing only on globally averaged attribution measures, such as the commonly used Pearson correlation coefficient, this paper extends to detailed temporal (localized in time) fingerprints of the North-Atlantic and Arctic oscillation patterns on the observed precipitation series. The Signal-to-Noise ratio (S-N ratio) was used to quantify the effects of the studied climatic indices on rainfall and new snow.

The purpose of this paper is twofold: first, to investigate the temporal effects of the AO and NAO on rainfall and new snow; second, to investigate the spatial patterns of affected stations located within the western portion of the Carpathian Mountains and a part of the adjacent Pannonian Plain.

2. Materials and methods

2.1. Study area and data

The western Carpathians and the adjacent Pannonian plain are located in central Europe, as shown in Fig. 1. For the purposes of this study, we used monthly data on precipitation and new snow. All data were obtained from the national weather service (Slovak Hydrometeorological Institute) and underwent standard quality control.

New snow is defined here as a snowpack accumulated over the previous 24 hours prior to measurement at 0700 Local Mean Time. The monthly values of new snow were calculated as a sum of new snow daily recordings. Similarly, the monthly values of precipitation are the sum of all daily observations of precipitation (both liquid water and ice/snow in winter). The time series of monthly rainfall totals and new snow were obtained from the

databases of the national hydrometeorological service (Slovak Hydrometeorological Institute, Bratislava, Slovakia). The precipitation and snow cover a period of ~ 36 years. In total, we analysed 177 rainfall series and 33 snowpack series.

Monthly values of the AO were obtained from the Regional Climate Center at KNMI via the Climate Explorer located at `https://climexp.knmi.nl/`. The station-based NAO indices produced by NCAR's Climate Analysis Section were downloaded as an ASCII text file from Hurrell North Atlantic Oscillation (NAO) Index (station-based) | NCAR – Climate Data Guide (`https://www.ucar.edu/`). This index is based on the paper of *Hurrell (1995)*. The NAO index was calculated for each station's raw sea level pressure data, normalized each month separately by the long-term mean over the period of 1864–1983. The pressure at the northern station (Reykjavik) was then subtracted from the southern station (Ponta Delgada). The monthly climatic indices NAO and AO were downloaded from the Climate Explorer located at `https://climexp.knmi.nl/`.

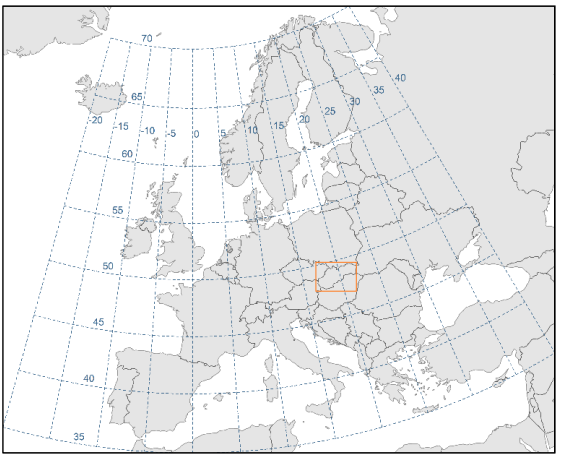

Fig. 1. Location of the investigated region: the western part of the Carpathians Mountains and the adjacent Pannonian Plain.

2.1.1. Data analyses

A comprehensive flowchart describing the procedure we followed in this paper is presented in Fig. 2. First, it was necessary to calculate the con-

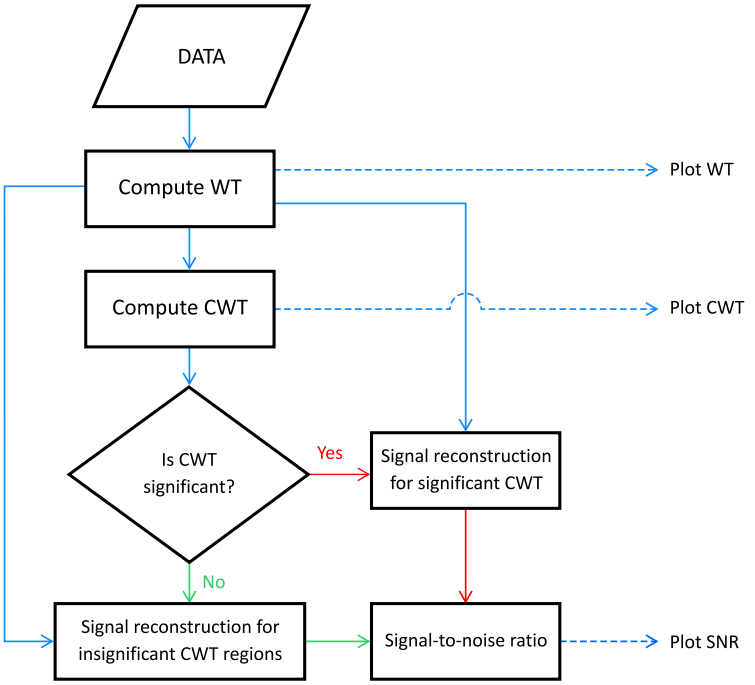

Fig. 2. Flowchart representing the structure of data analyses.

tinuous wavelet transform for the observed time series of rainfall and new snow. The climatic indices (NAO and AO) were used as covariates for the wavelet-coherence transform. As originally described in *Torrence and Compo (1998)*, for a series of observations x_n the wavelet transform is defined as a convolution of x_n with a scaled and translated wavelet basis function $\Psi_0(\eta)$:

$$W_n(s) = \sqrt{\frac{t}{s}} \sum_{n'}^{N-1} x_n \, \Psi * \left[\frac{(n' - n)\, \delta t}{s} \right], \tag{1}$$

where Ψ is the wavelet basis function (mother wavelet) that depends on a non-dimensional time parameter η. The wavelet power is the squared absolute value of the wavelet transform $|W_n^Y(s)|^2$ (*Grinsted et al., 2004*). By stretching the wavelet in the time domain (i.e. varying the scale s) so that $\eta = std$, a set of different wavelet basis can be obtained. The wavelet transform can be viewed as a band-pass filter in which the time series (x_n)

is convolved with the scaled and normalized wavelets (*Duan et al., 2018; Grinsted et al., 2004*). We applied the Morlet basis function, which is far the most common basis function used in geosciences (e.g. *Onderka and Chudoba, 2018; Duan et al., 2018; Rashid et al., 2016; Grinsted et al., 2004*).

Our goal was to decompose the signal into time-frequency space and identify noise-related time-frequency regions within the CWT. Furthermore, we used the CWT to identify co-varying time-frequency regions related to the climatic indices. A de-noising mask was generated by setting the wavelet coefficients outside the significant coherent time-frequency regions of the wavelet transform to zero. The wavelet energy of signals other than the climatic indices AO and NAO was suppressed by applying the previously created mask to the wavelet coefficients. Finally, the signal related to NAO and AO was reconstructed using the inverse wavelet transform (Eq. (2)).

One of the advantages of wavelet transform is that the wavelet coefficients can be used to reconstruct the original signal x_{rec}:

$$x_{rec} = \frac{\delta j \, \delta t^{1/2}}{C_\delta \, \Psi_0(0)} \sum_{j=0}^{J} \frac{\mathrm{real}\{W_n(s_j)\}}{s_j^{1/2}} \,, \tag{2}$$

where $\Psi_0(0)$ is a factor to remove the energy scaling, $s^{1/2}$ converts the wavelet transform to an energy density; C_δ is an empirically derived constant with a values of 0.776 for the Morlet basis function (*Torrence and Compo, 1998*). Equation (2) can be thought of as a band-pass filter when used for a sub-set of scales or for both the scale and time simultaneously by defining a threshold of e.g. wavelet power, cross-wavelet transform, or wavelet coherence. In our approach we used the wavelet coherence to define regions of significant common power (coherent spectra) to filter out the "signal" and the "noise" from the time series. This technique removes noise at all frequencies and can be used to identify individual events with varying frequencies (*Torrence and Compo, 1998*).

Another important piece of information that can be extracted from wavelet analysis is the wavelet coherence. Similar to the traditional Spearman correlation coefficient, the wavelet coherence always takes values between zero and unity. The coherence spectrum shows how strongly two signals are correlated across a wide range of frequencies because its definition closely resembles that of a traditional correlation coefficient (*Schulte et al., 2016; Grinsted et al., 2004*):

$$R_n^2(s) = \frac{\left|S\left(s^{-1}W_n^{XY}(s)\right)\right|^2}{S\left(s^{-1}\left|W_n^X(s)\right|^2\right)\, S\left(s^{-1}\left|W_n^Y(s)\right|^2\right)}\,, \tag{3}$$

where S is a smoothing operator, $|W_n^X(s)|^2$ is the wavelet power of time series X, and $|W_n^Y(s)|^2$ is the wavelet power of the time series Y, and finally $W_n^{XY}(s)$ is the cross-wavelet of the two time series X and Y. A detailed description of the cross-wavelet transform $W_n^{XY}(s)$ can be found in the relevant literature (e.g. *Torrence and Compo, 1998; Grinsted et al., 2004*). The spectral coherence between time series of NAO, AO and precipitation (rainfall and new snow) is used in this study to identify regions where two investigated signals are mutually coherent (or correlate in time).

2.1.2. Signal-to-Noise ratio

The Signal-to-Noise ratio (S-N ratio) is defined as the squared ratio of the signal variance σ_{signal} to the noise variance σ_{noise}. The term "signal", for the sake of this paper, is defined a significantly coherent portion of the observed variable Y (rainfall or snowfall) with the covariate X(i.e. NAO or AO). The term "noise" refers to all signals that are not related to the considered climatic indices (NAO and AO). The S-N ratio is mathematically expressed as:

$$SNR = \frac{\sigma_{signal}^2}{\sigma_{noise}^2}\,. \tag{4}$$

The S-N ratio (Eq. (4)) was calculated for statistically only significant regions of the cross-wavelet spectrograms. Note, that variance σ is defined as the sum of signal departures from the mean divided by the standard deviation $(y_n - m)/std$, but in our calculations, the mean is zero because the reconstructed signal has a zero mean.

3. Results

Temporal patterns

First, we focused on the wavelet spectra of the long-distance drivers of precipitation variability, specifically using the NAO and AO indices. The time series of these two indices and their corresponding wavelet spectra are depicted in Fig. 3, where distinct features delineated by areas of high spectral

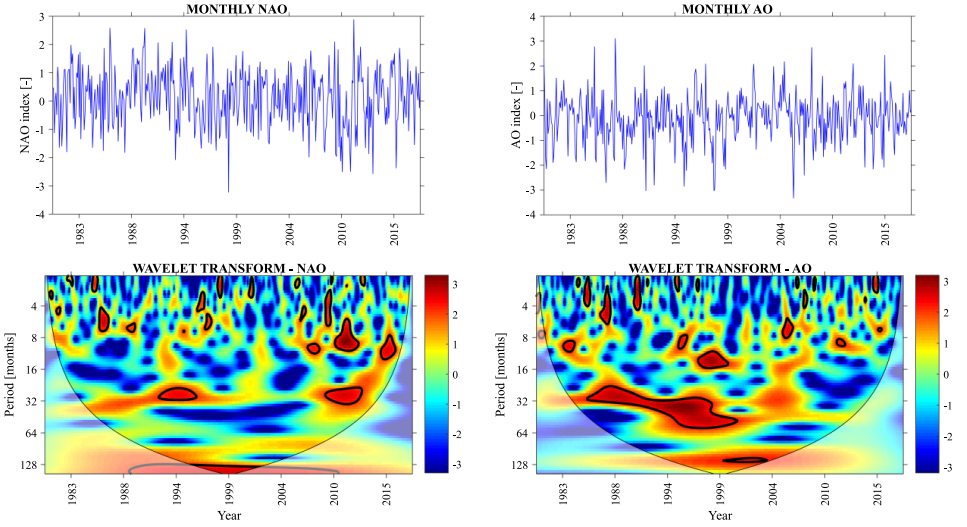

Fig. 3. Time series of monthly Arctic Oscillation index (AO) and the North Atlantic Oscillation index (NAO) over the period 1981–2017. The corresponding spectrograms of CWT are displayed below each time series. Note that the wavelet transform is not completely localized in time, leading to the presence of edge artefacts delineated by a 'cone of influence', where edge effects cannot be ignored.

power are evident. As indicated by the wavelet spectra, these areas of high spectral power exhibit interruptions over time. Some years show high spectral power, followed by years with spectral lows. This interrupted pattern in the power spectra is an intriguing observation, particularly when considering the conventional notion of periodicity known from Fourier spectra. Although Fourier analyses were not performed explicitly in the paper, we estimated the global wavelet spectra (i.e. averaging the wavelet spectral coefficient over the entire time scale), which can essentially be interpreted in the same way as Fourier spectra.

As shown in the global wavelet spectrograms in Fig. 4, the AO index exhibits strong annual (1−year), 3−year and 10−year periodicities, while the NAO index exhibits a strong annual periodicity and a periodicity at around 3 years.

As an illustrative example, we utilized a rainfall series collected from a specific rain gauge (Fig. 5) and performed the wavelet transform on its data. Upon initial examination, the wavelet power spectra of the rainfall reveal

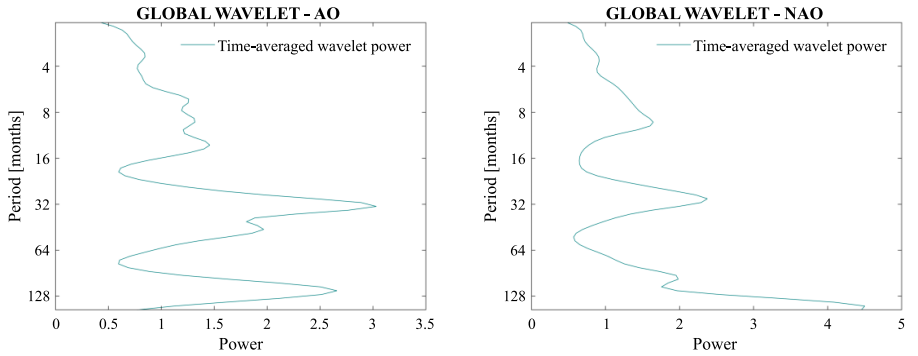

Fig. 4. Global wavelet power spectra (averaged in time) of the Arctic Oscillation index (left) and the North Atlantic Oscillation index (right). The dominant quasi−period in both spectrograms is located at $\sim 20-35$ months.

a considerably stronger annual signal in comparison to the NAO and AO indices (Fig. 3). However, the most intriguing aspect lies in the spectral coherence between the rainfall and the two indices. The coherence spectra, shown in Fig. 5, indicate periods of substantial common power and phase relationships between the two time series. To further analyse this coherence, we employed statistically significant regions in the coherence spectrograms as a filtering mask. This enabled the reconstruction of the precipitation signal, which, as we hypothesize, is influenced by the NAO and AO modes. Conversely, the regions with low coherence, deemed insignificant in the coherence spectrograms, were used to reconstruct the remaining portion of the rainfall signal and to calculate the signal-to-noise ratio. The resulting coherent rainfall signal exhibits some similarities with the isolated coherent structures seen in the coherence spectrogram (Fig. 5).

This procedure was also applied to the snow time series (Fig. 6), where the coherence spectra exhibit a robust annual pattern, characterized by more distinct temporal features. Notably, the strongest snow signal associated with the AO mode is observed at the beginning of the years 1985, 1993, and 2012 (Fig. 6), which coincide with the reported snowfall extremes.

Areal patterns

The areal distribution of signal-to-noise ratios, calculated for monthly rainfall and snowfall totals, along with the two indices, is presented in Figs. 7, 8, 9, and Fig. 10. When considering the annual totals of rainfall, the influ-

ence of the NAO mode on the monthly rainfall variability is most prominent from December through June, whereas the impact on summertime rainfall appears negligible (Fig. 7). Similarly, in the case of the AO, its attribution is evident, but the period of influence is shorter, mainly extending from June to July during early summer (Fig. 8). For snowfall analysis, the focus is limited to the snow season (DJF) since this period corresponds to when snowfall is typically observed in the Western Carpathians region under investigation. Analyzing the effects of NAO and AO on new snowpack

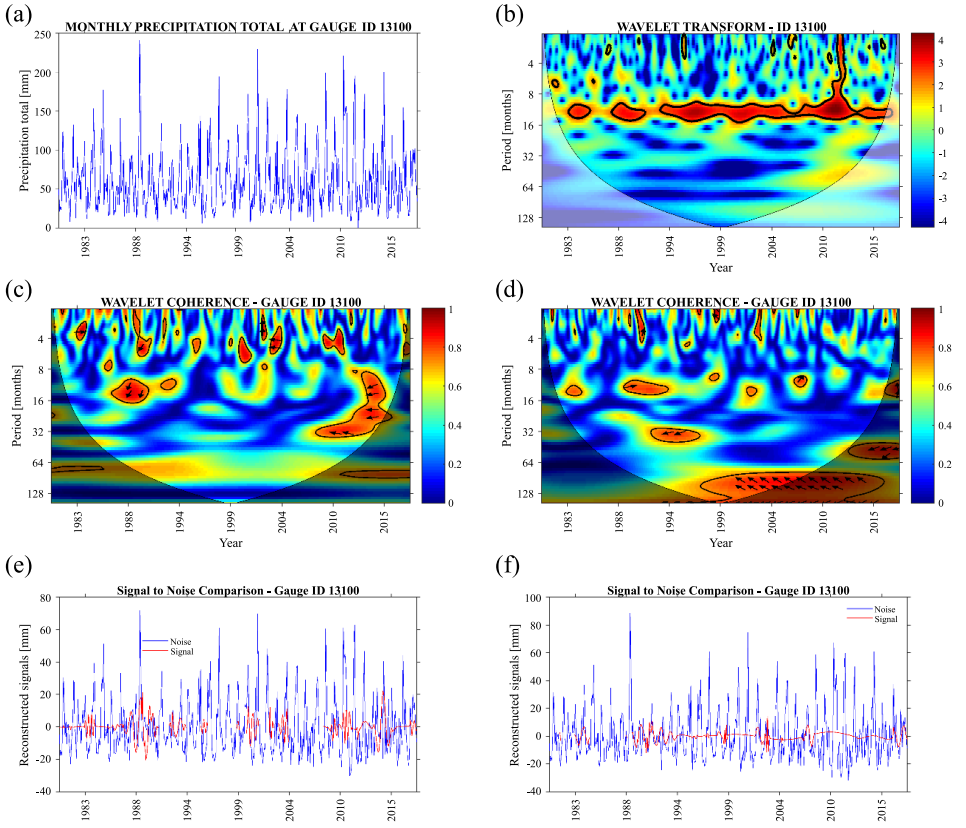

Fig. 5. An example of rainfall series observed at the Gauge No. 13100 (station name: Podolinec; latitude = 49°15′18″; longitude = 20°32′0″; elevation = 563 m a.s.l.). (a) wavelet spectra of monthly rainfall totals (b); wavelet coherence spectra between monthly rainfall totals and NAO (c) and AO (d); the relative contribution of NAO (e) and AO (f) to the coherent portion of the total rainfall signal.

in the summer would not be meaningful. The AO oscillation exhibits significant attribution to the overall variability of new snowpack, primarily in the eastern portion of the investigated region. As the winter season progresses toward spring, the AO gradually starts to affect a larger portion of the studied area (Fig. 9). In contrast, the NAO seems to impact only the southern part of the investigated area, particularly at the end of the snow season (specifically the Pannonian Plain south of the Western Carpathian mountains) as depicted in Fig. 10.

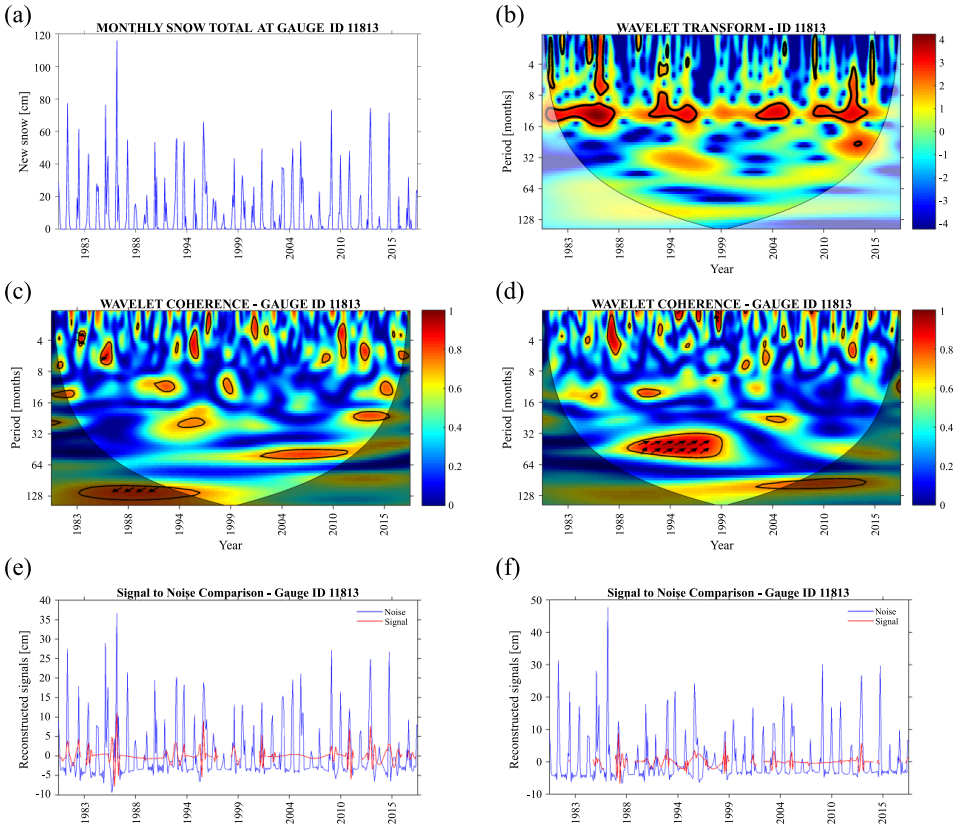

Fig. 6. An example of time series of new snowpack observed at the Gauge No. 11813 (station name: Bratislava−Koliba; latitude = 48°10′7″; longitude = 17°6′38″; elevation = 287 m a.s.l.). (a) wavelet spectra of monthly snowpack (b); wavelet coherence spectra between monthly snowpack and NAO (c) and AO (d); and the relative contribution of NAO (e) and AO (f) to the coherent portion of the snowpack series.

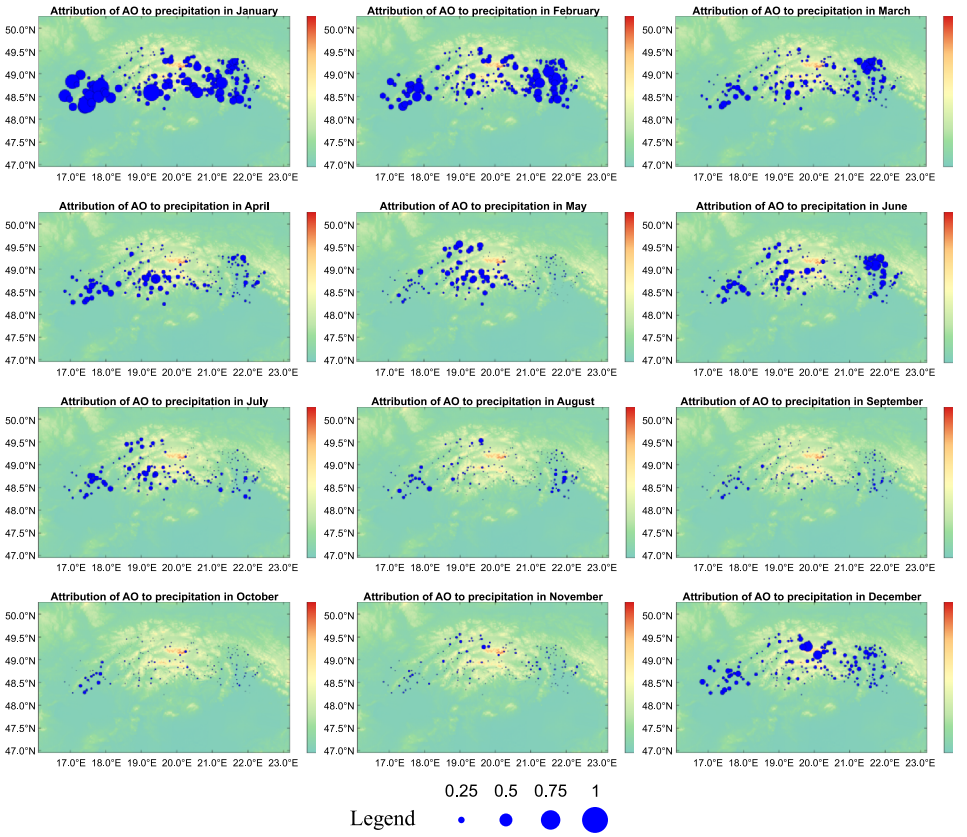

Fig. 7. Areal distribution of signal-to-noise ratio determined for monthly rainfall totals and Arctic Oscillation index.

4. Discussion and conclusions

We analysed influence of two major atmospheric oscillation modes, namely the North Atlantic Oscillation (NAO) and the Arctic Oscillation (AO), on the temporal and spatial variability of monthly rainfall totals and new snowpack in the western part of the Carpathians and the adjacent Pannonian Plain. The temporal and spatial patterns of NAO and AO-related signal variance in monthly rainfall totals and new snowpack was evaluated on ground-based observations (station data) on a monthly basis. Our findings revealed varying degrees of contribution by the NAO and AO to the intra-

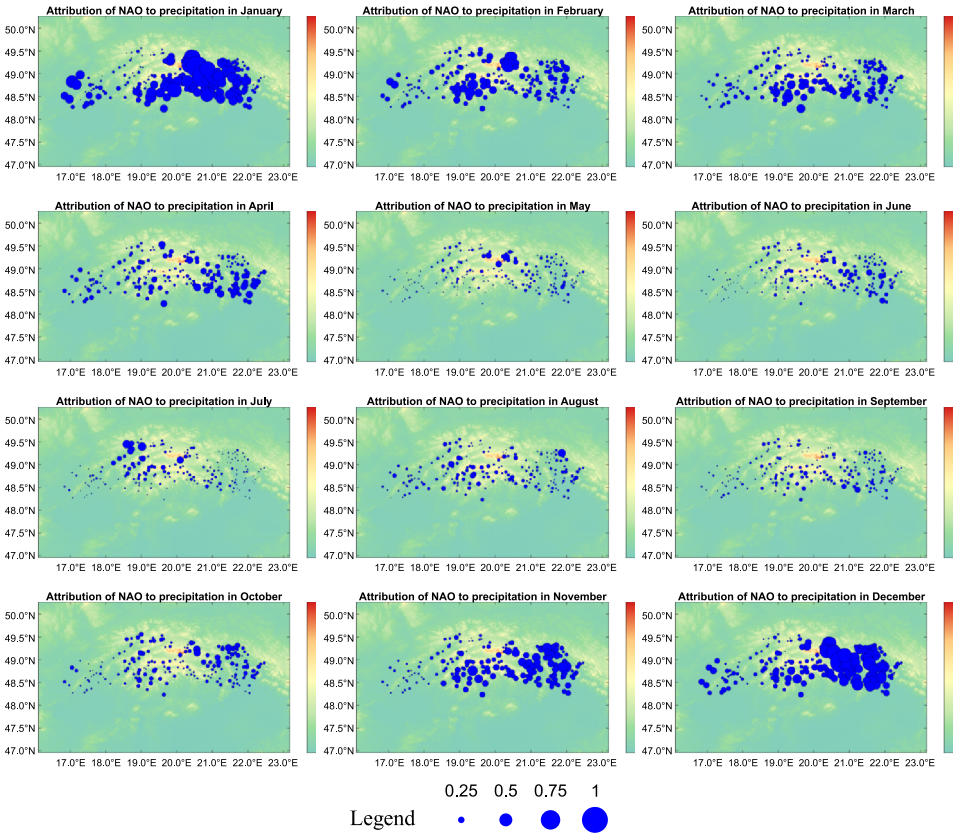

Fig. 8. Areal distribution of signal-to-noise ratio determined for monthly rainfall totals and North atlantic Oscillation index.

annual variability of monthly rainfall totals and new snowpack in the investigated region. Using wavelet analyses, we showed that historical snowfall extremes and the overall variability of monthly cumulative new snowpack depth were largely attributable to the variability of the North Atlantic Oscillation. Notably, the NAO mode played a significant role in major observed snow calamities. For example, in January 1985, Europe experienced an extremely cold and snowy month following a warm December of 1984. Central and southern Europe, including the investigated region, were impacted by heavy snowfall, marking the beginning of a prolonged cold wave with extremely low air temperatures across the continent. Similarly, in 2012,

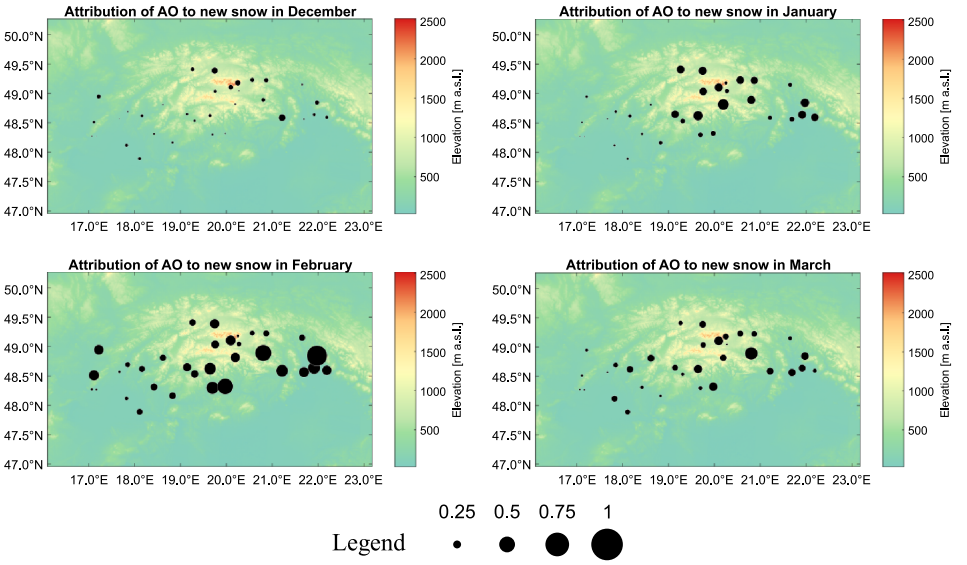

Fig. 9. Areal distribution of signal-to-noise ratio determined for new snowpack and Arctic Oscillation index.

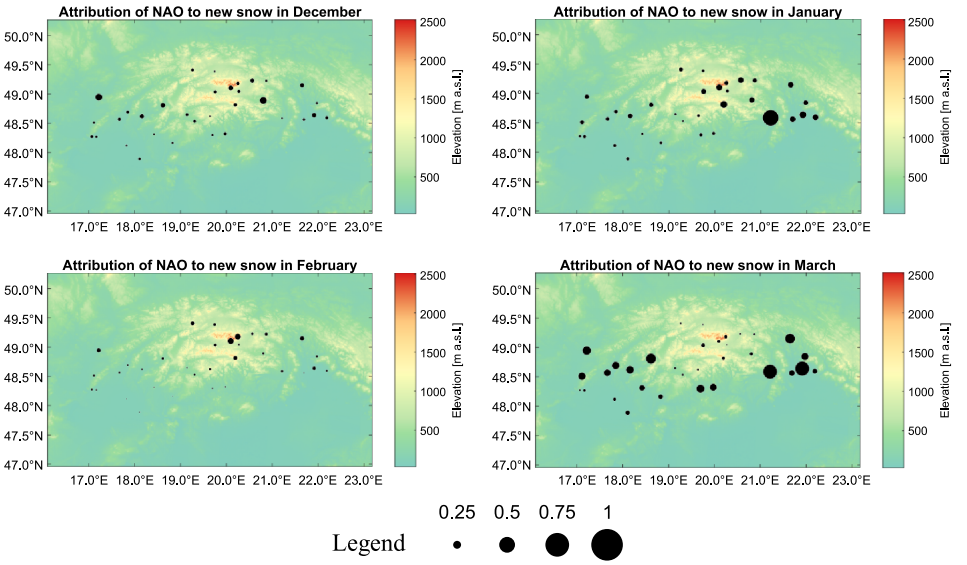

Fig. 10. Areal distribution of signal-to-noise ratio determined for rainfall totals and North Atlantic Oscillation index.

a notable snowfall event affected the northern part of Europe, with heavy snowfall observed in the second half of January 2012, leading to new snowpack reaching up to 1m, significantly impacting Slovakia and Bulgaria. In contrast, our analyses indicated that the AO mode had only a limited effect on the overall variability of new snowpack in late winter. When it comes to the variability of monthly rainfall totals, the attribution of NAO and AO modes was found to be less pronounced compared to their influence on new snowpack variability.

Acknowledgements. The research presented in this paper would not be possible without the following grants: "Scientific support of climate change adaptation in agriculture and mitigation of soil degradation" (ITMS2014 + 313011W580), supported by the Integrated Infrastructure Operational Programme and funded by the ERDF; and the national VEGA grant No. 2/0003/21 "Complex analysis of the effects of rising air temperature on rainfall extremes in Slovakia".

References

Bednorz E., Wibig J., 2008: Snow depth in eastern Europe in relation to circulation patterns. Ann. Glaciol., **48**, 135–149, doi: 10.3189/172756408784700815.

Brands S., Herrera S., Gutiérrez J., 2014: Is Eurasian snow cover in October a reliable statistical predictor for the winter climate on the Iberian Peninsula? Int. J. Climatol., **34**, 5, 1615–1627, doi: 10.1002/joc.3788.

Casanueva A., Rodríguez-Puebla C., Frías M. D., González-Reviriego N., 2014: Variability of extreme precipitation over Europe and its relationships with teleconnection patterns. Hydrol. Earth Syst. Sci., **18**, 2, 709–725, doi: 10.5194/hess-18-709-2014.

Duan L., Zhao Z., Lin Y., Wu X., Luo Y., Xu P., 2018: Wavelet-based method for removing global physiological noise in functional near-infrared spectroscopy. Biomed. Opt. Express, **9**, 8, 3805–3820, doi: 10.1364/BOE.9.003805.

Felsdstein S. B., 2000: The timescale, power spectra, and climate noise properties of teleconnection patterns. J. Clim., **13**, 24, 4430–4440, doi: 10.1175/1520-0442(2000)013<4430:TTPSAC>2.0.CO;2.

Fye K. F., Stahle D. W., Cook E. R., Cleaveland M. K., 2006: NAO influence on subdecadal moisture variability over central North America. Geophys. Res. Lett., **33**, 15, L15707, doi: 10.1029/2006GL026656.

Grinsted A., Moore J. C., Jevrejeva S., 2004: Application of the cross wavelet transform and wavelet coherence to geophysical time series. Nonlinear Process. Geophys., **11**, 5/6, 561–566, doi: 10.5194/npg-11-561-2004.

Hurrell J. W., 1995: Decadal Trends in the North Atlantic Oscillation: Regional Temperatures and Precipitation. Science, **269**, 5224, 676–679, doi: 10.1126/science.269.5224.676.

Onderka M., Chudoba V., 2018: The wavelets show it – the transit time of water varies in time. J. Hydrol. Hydromech., **66**, 3, 295–302, doi: 10.2478/johh-2018-0001.

Peings Y., Douville H., Colin J., Saint Martin D., Magnusdottir G., 2017: Snow–(N)AO Teleconnection and Its Modulation by the Quasi-Biennial Oscillation. J. Clim., **30**, 24, 10211–10235, doi: 10.1175/JCLI-D-17-0041.1.

Rashid M. M., Beecham S., Chowdhury R. K., 2016: Statistical downscaling of rainfall: a non-stationary and multi-resolution approach. Theor. Appl. Climatol., **124**, 3-4, 919–933, doi: 10.1007/s00704-015-1465-3.

Ríos-Cornejo D., Penas Á., Álvarez-Esteban R., del Río S., 2015: Links between teleconnection patterns and precipitation in Spain. Atmos. Res., **156**, 14–28, doi: 10.1016/j.atmosres.2014.12.012.

Rust W., Bloomfield J. P., Cuthbert M. O., Corstanje R., Holman I. P., 2021: Non-stationary control of the NAO on European rainfall and its implications for water resources management. Hydrol. Process., **35**, 3, e14099, doi: 10.1002/hyp.14099.

Schulte J. A., Najjar R. G., Li M., 2016: The influence of climate modes on streamflow in the Mid-Atlantic region of the United States., J. Hydrol. Reg. Stud.,**5**, 80–99, doi: 10.1016/j.ejrh.2015.11.003.

Seager R., Liu H., Kushnir Y., Osborn T. J., Simpson I. R., Kelley C. R., Nakamura J., 2020: Mechanisms of winter precipitation variability in the European-Mediterranean region associated with the North Atlantic oscillation. J. Clim., **33**, 16, 7179–7196, doi: 10.1175/JCLI-D-20-0011.1.

Tabari H., Willems P., 2018: Lagged influence of Atlantic and Pacific climate patterns on European extreme precipitation. Sci. Rep., **8**, 5748, doi: 10.1038/s41598-018-24069-9.

Torrence C., Compo G. P., 1998: A Practical Guide to Wavelet Analysis. Bull. Am. Meteorol. Soc., **79**, 1, 61–78, doi: 10.1175/1520-0477(1998)079<0061:APGTWA>2.0.CO;2.

Wang L., Ting M., Kushner P. J., 2017: A robust empirical seasonal prediction of winter NAO and surface climate. Sci. Rep., **7**, 279, doi: 10.1038/s41598-017-00353-y.